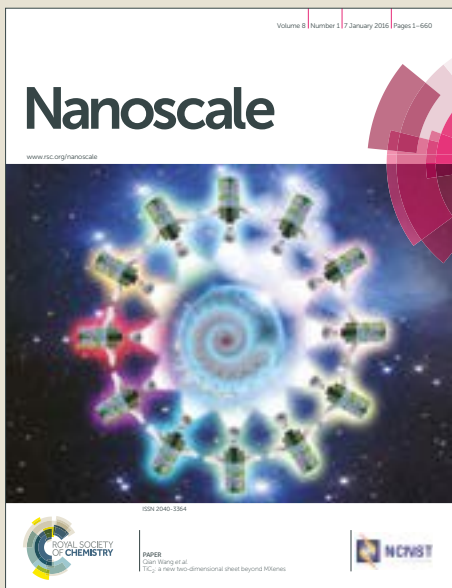


Nanoscale

Accepted Manuscript

This article can be cited before page numbers have been issued, to do this please use: B. Narayanan, H. Chan, A. Kinaci, F. G. Sen, S. Gray, M. Chan and S. Sankaranarayanan, *Nanoscale*, 2017, DOI: 10.1039/C7NR06038F.



This is an Accepted Manuscript, which has been through the Royal Society of Chemistry peer review process and has been accepted for publication.

Accepted Manuscripts are published online shortly after acceptance, before technical editing, formatting and proof reading. Using this free service, authors can make their results available to the community, in citable form, before we publish the edited article. We will replace this Accepted Manuscript with the edited and formatted Advance Article as soon as it is available.

You can find more information about Accepted Manuscripts in the [author guidelines](#).

Please note that technical editing may introduce minor changes to the text and/or graphics, which may alter content. The journal's standard [Terms & Conditions](#) and the ethical guidelines, outlined in our [author and reviewer resource centre](#), still apply. In no event shall the Royal Society of Chemistry be held responsible for any errors or omissions in this Accepted Manuscript or any consequences arising from the use of any information it contains.

Journal Name

ARTICLE TYPE

Cite this: DOI: 10.1039/xxxxxxxxxx

Received Date

Accepted Date

DOI: 10.1039/xxxxxxxxxx

www.rsc.org/journalname

Machine learnt bond order potential to model metal-organic (Co-C) heterostructures

Badri Narayanan,^{*a‡} Henry Chan,^a Alper Kinaci,^a Fatih G. Sen,^a Stephen K. Gray,^a Maria K. Y. Chan,^a and Subramanian K. R. S. Sankaranarayanan^{*a}

A fundamental understanding of the inter-relationships between structure, morphology, atomic scale dynamics, chemistry, and physical properties of mixed metallic-covalent systems is essential to design novel functional materials for applications in flexible nano-electronics, energy storage and catalysis. To achieve such knowledge, it is imperative to develop robust and computationally efficient atomistic models that describe atomic interactions accurately within a single framework. Here, we present a unified Tersoff-Brenner type bond order potential (BOP) for Co-C system, trained against lattice parameters, cohesive energies, equation of state, and elastic constants of different crystalline phases of cobalt as well as orthorhombic Co₂C derived from density functional theory (DFT) calculations. The independent BOP parameters are determined using a combination of supervised machine learning (genetic algorithms) and local minimization via the simplex method. Our newly-developed BOP accurately describe the structural, thermodynamic, mechanical, and surface properties of both the elemental components as well as the carbide phases, in excellent accordance with DFT calculations and experiments. Using our machine-learnt BOP potential, we performed large-scale molecular dynamics simulations to investigate the effect of metal/carbon concentration on the structure, and mechanical properties of porous architectures obtained via self-assembly of cobalt nanoparticles and fullerene molecules. Such porous structures have implications in flexible electronics, where materials with high electrical conductivity and low elastic stiffness are desired. Using unsupervised machine learning (clustering), we identify the pore structure, pore-distribution, and metallic conduction pathways in self-assembled structures at different C/Co ratios. We find that as the C/Co ratio increases, the connectivity between Co nanoparticles becomes limited, likely resulting in low electrical conductivity; on the other hand, such C-rich hybrid structures are highly flexible (i.e., low stiffness). The BOP model developed in this work is a valuable tool to investigate atomic scale processes, structure-property relationships, and temperature/pressure response of Co-C systems, as well as design organic-inorganic hybrid structures with desired set of properties.

1 Introduction

Transformative advances in flexible electronics, automobiles, aviation, catalysis, and energy storage technologies require multi-functional materials with properties that often conflict with each other.^{1–4} Such a conflicting set of properties/functionalities (e.g., a combination of low density and high strength) cannot be achieved with traditional materials containing single components alone, which in turn, pose a grand materials design challenge.¹

One possible route to address this pressing issue is to develop new hybrid materials that are composed of both organic and inorganic components, each with different functionalities.^{5–7} For instance, porous metal-organic hybrid materials hold promise for flexible electronics; in these heterostructures, the metallic component provides electric conduction pathways, while the organic counterpart confers the desired flexibility.^{3,8} These organic/inorganic hybrid materials also offer a unique opportunity to achieve exotic combinations of physical, chemical, mechanical, optical and electrical properties via engineering the nanoscale interfaces between the various components.^{9–12} Such interfaces are commonly found in biological systems, and have also been previously exploited in numerous artificially developed materials.^{13–17} A few representative examples include (a) biominerals

^a Center for Nanoscale Materials, Argonne National Laboratory, Lemont, IL, 60439, USA

[‡] Present Address: Materials Science Division, Argonne National Laboratory, Lemont, IL, 60439, USA

* Corresponding authors. Email: bnarayanan@anl.gov, skrssank@anl.gov

such as bones or teeth, in which the buried organic/inorganic interfaces provide the necessary fracture toughness and wear resistance,¹⁸ (b) inorganic nanomaterials functionalized with organics, which are promising for medical or sensing applications,^{19,20} (c) thin organic film coatings on LiFePO₄ electrodes in lithium ion batteries to improve electrode conductivity,²¹ (d) solid electrolyte interphases that form near the electrodes of Li-ion batteries, and control the cycling performance of the battery,²² and (e) metal/organic as well as oxide/polymer interfaces with key applications in dye-sensitized solar cells, organic photovoltaics, nano-dielectrics for organic field-effect transistors, and flexible electronic displays.^{23,24}

Among the organic/inorganic hybrid materials, porous hierarchical architectures made up of transition metal nanoparticles (e.g., Co) and carbonaceous material (e.g., carbon binder) have attracted a lot of attention for various technological applications, including, catalysis, flexible opto-electronics, magnetic devices, and energy storage.^{3,25–29} Additionally, nanoscale metal-carbon (e.g., cobalt-carbon) interfaces are also relevant for various chemical processes, such as, ammonia synthesis from N₂, Fischer-Tropsch process for producing hydrocarbons from H₂ and CO, and carbon nanotube formation.^{30–32} Despite their technological importance and significant advances in the synthesis protocols for metal-organic hybrid hetero-structures, several questions pertaining to the chemistry, atomic structure, and dynamical processes at the metal-carbon interface still remain unanswered. For instance, a few open questions include (a) the principal atomic-scale forces that govern the growth of metal-organic hybrid structures and the final architecture of the assembly, (b) stability of the assembled structure, (c) dependence of the pore morphology on the size/shape of metal nanoparticles, and carbon content, and (d) relationship between morphology of the aggregate porous structure and its physical properties. A fundamental understanding of these interfaces, especially at the atomic length scale, is crucial to enable precise control over processing parameters, structure, and performance of the final assembled multi-functional hybrid material. Molecular dynamics (MD) simulations based on classical interatomic potentials provide an ideal route to achieve such knowledge, since they can access the necessary length- (tens of nm), and time-scales (several ns).^{33–35}

The chemical complexity of the metal-organic interfaces presents a significant challenge in developing potentials or empirical force fields (EFFs) that accurately describe the atomic interactions. In particular, at metal-organic interfaces, the nature of the chemical environment ranges from metallic (in metal-rich regions) to covalent (in the organic-rich regions). Such diverse chemical bonding characteristics are often difficult to accurately and efficiently treat within a single potential formalism. It is a common practice in the literature to employ different potential models to describe the interatomic interactions in regions with a given bonding character (metallic, ionic or covalent). For example, the embedded atom method (EAM) is used to describe interactions between metal atoms, in which an effective local electron density term is added to pairwise interactions.³⁶ On the other hand, bond order models such as Tersoff and reactive empirical bond-order (REBO) are used to describe the covalent inter-

actions in carbon or organic materials.^{37–39} The interfacial region where the bonding character changes (e.g. from metallic to covalent) is, however, usually, described by pairwise dispersion terms (e.g. Lennard-Jones potential using Lorentz-Berthelot mixing rules).⁴⁰ A few previous works describe metal-carbon interactions via spherically symmetric terms dependent on local density, while neglecting angular effects (e.g., Shibuta potential).⁴¹ Such approaches often do not adequately capture the interfacial structure and properties, either due to the limited scope of the functional form of the EFF (e.g., lack of 3-body terms^{42,43}), or the use of a restricted set of training data (e.g., only up to 4-atom clusters for Shibuta potential⁴¹). It is, thus, desirable to describe the metal-organic heterosystems within a single potential formalism that can account for both metallic, and covalent interactions.

One such formalism is the reactive force field (ReaxFF), which captures the atomic bond-orders (chemical bonding environment) via local atomic coordination, and allows for dynamic charge transfer between atoms. Consequently, ReaxFF provides an accurate description of bond formation/dissociation, chemical reaction pathways, and transition states in a diverse class of materials, including metals, hydrocarbons, nitrides and oxides.^{44–46} ReaxFF is, however, extremely complex, involving a large number of parameters, and is computationally expensive, especially for large system sizes (millions of atoms) necessary to study metal-organic interfaces. While ReaxFF type models may be necessary for describing heterosystems with ionic bonding such as oxides, cheaper alternatives are desirable for systems, especially metallic-covalent systems, with no significant charge transfer. Bond order potentials (BOP) utilizing the Tersoff-Brenner formalism^{37,38,47} represent a viable alternative. Although such nearest-neighbor models have been traditionally used to describe covalent materials, such as C and Si,^{37,38} the BOP formalism has been successfully employed to model a variety of metals (e.g. Au, Fe) as well.^{42,43,48} Evidently, BOP provides a unique opportunity to describe directional (covalent) as well as metallic bonding within a unified, yet robust and computationally-efficient framework.

Here, we present a first principles based unified BOP model for describing metallic (Co-Co), covalent (C-C), and mixed (Co-C) interactions in a representative organic-inorganic heterosystem, namely, cobalt-carbon. Using supervised machine learning approach, we train this model against lattice constants, internal coordinates, elastic constants, cohesive energies and surface energies for condensed phases of pure cobalt, pure carbon, and cobalt carbide, as derived from density functional theory (DFT) calculations. Specifically, we employ a combination of genetic algorithms (GA), and local minimization via simplex to optimize the independent BOP parameters for Co-C system; this approach is motivated by our recent successes in employing multi-level evolutionary optimization methods for developing accurate EFFs^{42,49–52} Our machine learnt BOP accurately predicts structural, mechanical, and energetic properties of pure cobalt, pure carbon, as well as mixed interfacial phases; consequently, this model is well-equipped to provide insights into atomic-scale processes and structure-property relationships in Co-C heterosystems. Additionally, the predictive power of this model makes it suitable to computationally engineer new Co/C architectures with

desired set of properties.

This paper is organized as follows: Section 2 describes potential model formalism i.e., the Tersoff formalism, the training data set, and the parameterization strategies we employ for potential model development. Section 3 reports our results of the multi-level evolutionary optimization, the optimized Tersoff parameters for C-Co system obtained in this study, the structural and energetic properties predicted by these parameters, and their success in describing inter-atomic interactions in C-Co heterosystem. Section 4 provides a representative example illustrating the application of our newly developed Tersoff model, in which we perform large scale MD simulations of self-assembly of Co nanoparticles and C₆₀ fullerenes into porous architectures with implications in flexible electronics. These simulations show that the structural evolution as well as the elastic properties of the final assembled porous Co-C structure is strongly influenced by the relative compositions of C:Co. Specifically, we employed unsupervised machine learning algorithms (clustering) to analyze the pore distribution in the self-assembled structures obtained from MD simulations; these indicate that porous networks with low C:Co ratio exhibit higher stiffness, and possess high connectivity between Co clusters (with likely high electrical conductivity). Finally, Sec. 5 summarizes the key findings and provides concluding remarks.

2 Methods

2.1 Bond order potential

To model the interactions between Co and C atoms, we adopt the Tersoff-Brenner form^{37,38,47} of a bond-order potential (BOP). This formalism has been successfully employed to describe a diverse range of materials, including metals, ionic and covalent solids, as well as those with mixed bonding characteristics (e.g., Zn-O,⁵³ W-C⁵⁴). The details of the BOP scheme are available elsewhere;^{37,38} here, for the sake of completeness, we briefly summarize the key functions necessary to compute the potential energy of a given atomic configuration.

In the framework of Tersoff-Brenner BOP, the total potential energy V of a system composed of N atoms is defined as the sum of bond energy contributions arising from distinct pairs of atoms $i-j$, and is written as:³⁸

$$V = \sum_i^{N-1} \sum_{j>i}^N f_c(r_{ij}) [f_r(r_{ij}) + b_{ij} f_a(r_{ij})], \quad (1)$$

where $f_c(r_{ij})$, $f_r(r_{ij})$, and $f_a(r_{ij})$ are the cut-off function, pairwise repulsive and attractive bond energy terms respectively. Note that the indices i and j also monitor the atom types and consequently, the type-dependence of parameter values. The cut-off function limits the range of interactions to nearest-neighbors alone and is given by:³⁸

$$f_c(r_{ij}) = \begin{cases} 1 & : r_{ij} < R_{ij} \\ \frac{1}{2} - \frac{1}{2} \sin \frac{\pi}{2} \left(\frac{r_{ij}-R_{ij}}{S_{ij}-R_{ij}} \right) & : R_{ij} \leq r_{ij} < S_{ij} \\ 0 & : r_{ij} \geq S_{ij} \end{cases} \quad (2)$$

where R_{ij} and S_{ij} are adjustable parameters. The pairwise repulsive and attractive components of the bond energy between atoms

i and j have a Morse-like exponential dependence on separation distance:³⁸

$$f_r(r_{ij}) = A_{ij} e^{-\lambda_{ij}^{(1)} r_{ij}}, \quad (3)$$

$$f_a(r_{ij}) = B_{ij} e^{-\lambda_{ij}^{(2)} r_{ij}}, \quad (4)$$

where A_{ij} , B_{ij} , $\lambda_{ij}^{(1)}$, and $\lambda_{ij}^{(2)}$ are free parameters. The effect of local environment around a given atom pair $i-j$ on its bond energy is treated via bond order b_{ij} (Eq. 1). The value of this bond order depends on three-body interactions surrounding pair $i-j$, as given by:³⁸

$$b_{ij} = \left(1 + \beta_{ij}^{n_{ij}} \zeta_{ij}^{n_{ij}} \right)^{\frac{-1}{2n_{ij}}}, \quad (5)$$

$$\zeta_{ij} = \sum_{k \neq i,j} f_c(r_{ik}) g(\theta_{ijk}), \quad (6)$$

$$g(\theta_{ijk}) = 1 + \frac{c_{ij}^2}{d_{ij}^2} - \frac{c_{ij}^2}{d_{ij}^2 + (h_{ij} + \cos \theta_{ijk})^2}, \quad (7)$$

where β_{ij} , n_{ij} , c_{ij} , d_{ij} , and h_{ij} are independent parameters. In all, the BOP for Co-C system contains 33 independent parameters. Of these, we optimize 22 parameters (i.e., 11 for Co-Co, and 11 for Co-C interactions) while the remaining 11 parameters governing the C-C interactions are taken from earlier work by Tersoff (Ref. 38). By using C-C parameters provided by Tersoff,³⁸ we retain its well-known accuracy in describing the structure, thermodynamics, mechanical, and surface properties of various forms of carbon (including graphite, diamond, graphene, nanotubes, fullerenes etc.), each featuring distinct local atomic coordination.

2.2 Evolutionary strategy to optimize BOP parameters

We employ a combination of global optimization via genetic algorithms (GA) and local minimization (simplex method) to optimize the independent BOP parameters, namely, c , d , h , β , n , $\lambda^{(2)}$, B , R , S , $\lambda^{(1)}$, and A for Co-Co, and Co-C interactions (i.e., a total of 22 parameters); the overall procedure is outlined in Figure 1.

The first step towards the development of an accurate and transferable interatomic potential involves the use of a training set that constitutes a good sampling of the potential energy landscape. In this study, we employ density functional theory (DFT) calculations to derive a training set containing (a) equations of state, (b) lattice parameters, (c) cohesive energies, and (d) elastic constants of different crystalline phases of cobalt as well as Co₂C. For cobalt, we consider four stable and metastable polymorphs, namely hexagonal close packed (hcp), face-centered cubic(fcc), body-centered cubic (bcc), and diamond cubic. For cobalt carbides, we employ a metastable Co₂C phase with orthorhombic symmetry (space group: *Pnnm*) which has been previously reported to occur during Fischer-Tropsch synthesis.^{55–58}

All the DFT calculations are performed with plane wave basis and the projector-augmented wave formalism as implemented in the Vienna *ab initio* simulation package VASP.^{59,60} We describe the exchange correlation using the Perdew-Burke-Ernzerhof (PBE) generalized gradient approximation (GGA) functional,⁶¹ with the PAW pseudopotentials Co (valence: 3d⁸ 4s¹),

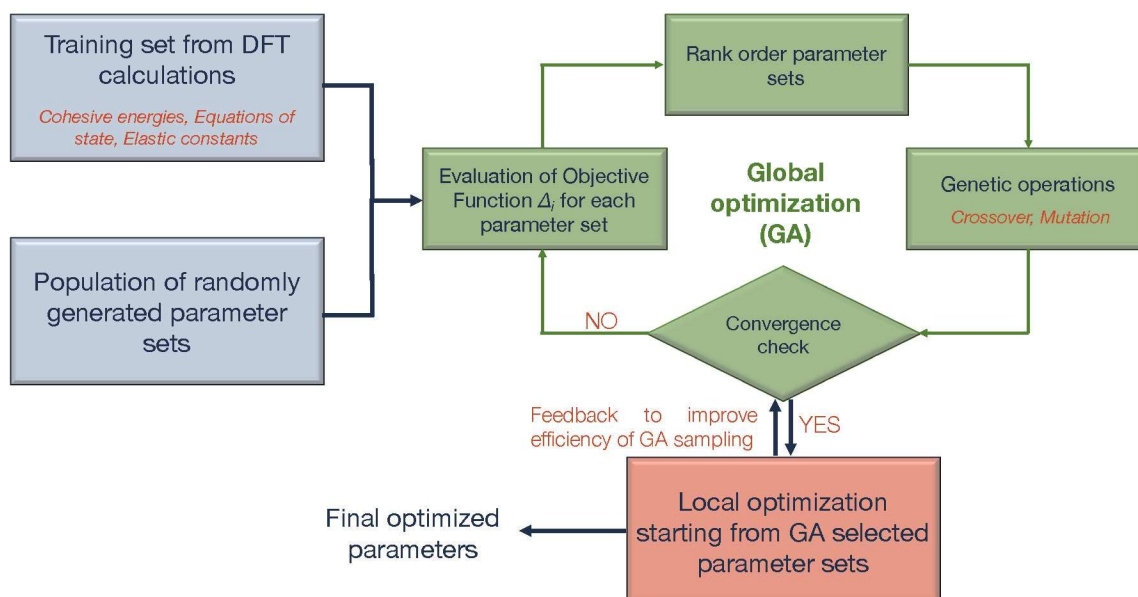


Fig. 1 Schematic representation of the evolutionary strategy that combines genetic algorithms and local minimization via the simplex method to parameterize bond order interatomic potential for Co-C system.

and C (valence: $2s^2 2p^2$), which are known to describe carbides well.^{59,60} The plane wave energy cutoff is set at 500 eV. The equations of state, cohesive energy, and structural optimization of each of the four crystalline polymorphs of Co, and orthorhombic Co₂C are calculated on a conventional unit cell. The Brillouin zone is sampled by Γ -centered Monkhorst-Pack grids. For Co phases, we use a k -point grid of $14 \times 14 \times 14$, while a $8 \times 6 \times 6$ k -point grid is selected for the orthorhombic Co₂C crystal. The atomic coordinates are relaxed using a conjugate gradient method until the force components on any atom are smaller than 0.01 eV/Å. The heat of formation of Co₂C is evaluated as $\Delta H = E_{\text{Co}_2\text{C}} - 2E_{\text{Co}} - E_{\text{C}}$, where $E_{\text{Co}_2\text{C}}$, E_{Co} , and E_{C} refer to the total energies of orthorhombic Co₂C, hcp Co, and graphite at equilibrium. In addition to the bulk calculations, we also computed energies of low-index surfaces of (a) hcp Co, namely, (0001) and (10\bar{1}0), as well as (b) fcc Co with orientations (001), (110), and (111). Note that these surface energies are not included in the training set used to fit the BOP parameters; they are rather used to test the performance of the obtained BOP parameters. The surface energy for a slab S with given surface orientation is obtained by subtracting the bulk energy E_b from the total energy of the slab E_s , that is, $\gamma = \frac{1}{2}(E_s - NE_b)$, where N is the number of atoms present in the slab. All surface calculations are performed on the smallest possible surface unit cell with seven layers in the direction normal to the slab; periodic boundary conditions are imposed in the plane of the slab, while a vacuum of 12 Å is included along the direction normal to the slab.

Once the training material properties are determined, we optimize the BOP parameters using an approach that uses a combination of genetic algorithms (for global sampling)⁶² and local minimization via the simplex method⁶³ (Figure 1). We begin the optimization procedure with a population of 100 randomly chosen BOP parameter sets (individuals); the values of these parameters

Table 1 Optimized BOP potential parameters obtained in this study.

	Co-Co	C-C ^a	Co-C
$c(\times 10^4)$	3.0611	3.8049	2.8062
d	113.064	4.384	95.0617
h	0.5289	0.5706	0.4961
β	0.0426	1.5724×10^{-7}	1.0
n	0.5916	0.7275	1.0
$\lambda^{(2)}(\text{\AA})$	1.3484	2.2119	0.6411
$B(\text{eV})$	80.5297	346.7	36.969225
$R(\text{\AA})$	2.85	1.8	1.9283
$S(\text{\AA})$	3.25	2.1	2.3283
$\lambda^{(1)}(\text{\AA})$	2.9699	3.4879	3.7166
$A(\text{eV})$	1017.1	1393.6	585.7

^a Ref. 38

are restricted within physically meaningful ranges. The fitness (or objective function) Δ_i of a particular individual i is determined by a weighted sum of squared errors in its predicted properties as compared to the DFT-derived training set; the higher the objective function value, the lower its fitness/ suitability. For each individual in the initial randomly chosen population, we evaluate all the material properties in the training set using the molecular dynamics package LAMMPS⁶⁴ to compute the objective function values. Next, we select individuals (parents) using a tournament selection without replacement method to perform crossover operation using simulated binary method.^{62,65,66} A fraction of the individuals are subjected to mutation via a polynomial of order 20.^{67,68} The probability of a crossover operation is set to 0.9, while that of mutation is 0.1. These mutations are necessary to maintain sufficient diversity in the population and, consequently, avoid premature convergence of the GA run. After the genetic operations, both the old (parents) and the newly-created individ-

Table 2 Lattice parameters, cohesive energy (E_c), and elastic constants C_{ij} of different polymorphs of cobalt using the BOP developed in this work. The corresponding values obtained from our DFT calculations, as well as experiments (when available) are provided for comparison. The absolute value of cohesive energy is provided only for the most stable polymorph, i.e., hexagonal close packed (hcp); for all other polymorphs, energies are listed relative to the hcp phase.

	BOP	DFT	Experiment
Hexagonal close-packed (Space Group: $P6_3/mmc$)			
E_c (eV/atom)	-4.38	-5.00	-4.39 ^a
a (Å)	2.51	2.49	2.51 ^b
c (Å)	4.07	4.03	4.07 ^b
C_{11} (GPa)	318	358	319 ^c
C_{12} (GPa)	119	164	166 ^c
C_{13} (GPa)	92	114	102 ^c
C_{33} (GPa)	346	409	374 ^c
C_{44} (GPa)	89	95	82 ^c
Face-centered cubic (Space Group: $Fm\bar{3}m$)			
ΔE_c (eV/atom)	0.0	0.02	0.84 ^d
a (Å)	3.53	3.54	3.54 ^e
C_{11} (GPa)	272	289	260 ^f
C_{12} (GPa)	129	173	160 ^f
C_{44} (GPa)	127	148	110 ^f
Body-centered cubic (Space Group: $Im\bar{3}m$)			
ΔE_c (eV/atom)	0.08	0.1	–
a (Å)	2.81	2.82	–
C_{11} (GPa)	216	143	–
C_{12} (GPa)	158	197	–
C_{44} (GPa)	154	108	–
Diamond cubic (Space Group: $Fd\bar{3}m$)			
ΔE_c (eV/atom)	0.83	1.25	–
a (Å)	5.08	5.07	–
C_{11} (GPa)	104	87	–
C_{12} (GPa)	60	69	–
C_{44} (GPa)	44	42	–

^aRef. 69; ^bRef. 70; ^cRef. 71; ^dRef. 72; ^eRef. 73; ^fRef. 74

uals (offspring) are ranked in decreasing order of their fitness, and the best 100 individuals are retained in the subsequent generation. This routine is repeated until the GA run does not result in any better individuals than the previous generation. To sufficiently sample the parameter landscape, we perform 10 different GA searches, each sampling a certain region of the parameter space (i.e., ranges of parameter values). To enhance the efficiency of the parameter sampling, we employ local optimization via Simplex⁶³ using the parameter sets identified by GA runs as starting guesses; feedback from these local optimization runs enables a relatively faster identification of regions of interest in the parameter space (i.e., those likely to contain parameter sets with low objective function), which are then searched by subsequent GA runs. Eventually, from the converged GA runs, we choose the best 20 unique individual (i.e., lowest objective functions); local minimization via Simplex⁶³ is then performed using these 20 parameters sets as starting guesses. We ensured that the 20 chosen starting guesses optimize to distinct local minima to avoid multiple initial guesses located preferentially in a certain region of the parameter space. The parameter sets from the converged Simplex runs are then assessed in terms of their objective function; the one with the lowest objective function is chosen as the final optimized set of BOP parameters. Note that, in addition to Simplex, we also tried two other local optimization methods, namely Levenberg-Marquardt⁶³ and POUNDERS;⁷⁵ these methods performed similar to Simplex. In essence, a scheme utilizing synergy between global optimization and local optimization methods enables efficient sampling of the parameter space, and performs better than using either of the techniques individually.

2.3 Molecular dynamics simulations of self-assembly of Co-C hybrid nanostructures

We performed large scale MD simulations using LAMMPS⁶⁴ in the framework of our newly developed BOP to investigate the self-assembly of Co nanoparticles and C₆₀ fullerenes at different compositions f , i.e., C/Co ratios. Each cobalt nanoparticle is simulated using a hcp bulk-truncated cluster composed of 515 atoms, while for fullerene molecules, we employ the C₆₀ configuration. Three different C/Co ratios are investigated, namely, $f = 0.086$, 0.429 and 4.292 . For each of these cases, initially 100 Co₅₁₅ clusters alongside desired number of C₆₀ molecules are placed at random locations separated by at least 3 Å in a computational supercell such that the overall number density is 23 atoms/nm³. Periodic boundary conditions are employed along all directions. Using the randomly packed initial configurations, we equilibrate the atomic systems at three different C/Co ratios at 800 K in a canonical ensemble for 2 ns; constant temperature conditions are maintained by employing the Nosé-Hoover thermostat as implemented in LAMMPS while a timestep of 0.5 fs is used to integrate the equations of atomic motion. The Young's moduli (elastic stiffness) of the final self-assembled structures are determined by computing the second derivative of total strain energy density with respect to applied strain following previous work.^{76–78}

3 Results and discussion

3.1 Performance of our newly developed BOP for Co-C

Using an evolutionary optimization technique (detailed in Figure 1), we determine the set of BOP parameters for Co-C system that best reproduces the DFT-derived training set containing structural, energetic, elastic, and surface properties of pure Co and Co_2C phases. These optimized BOP parameters are listed in Table 1. We have also provided these BOP parameters in a format readable by LAMMPS in the Supplementary Information.

Next, we assess the accuracy of our newly-parameterized BOP model (Table 1) by comparing its predictions for the physical properties of various polymorphs of Co, and Co_2C with our DFT calculations as well as previous experiments. Table 2 compares the BOP predicted cohesive energies, lattice parameters and elastic constants for five different polymorphs of Co with the values derived from our DFT calculations and experiments. In terms of energetics, we note that the cohesive energy values E_c of pure Co phases derived from DFT show a significant deviation from empirical measurements; e.g., as shown in Table 2, the DFT derived E_c for hcp Co (-5.0 eV/atom; consistent with previous report⁷⁹) is ~0.6 eV/atom away from experiments (-4.39 eV/atom). Despite this issue, DFT calculations have been previously reported to accurately capture the energetic differences between the various Co phases,⁸⁰ which are crucial for development of a robust interatomic potential. To avoid inheriting the DFT errors in cohesive energy descriptions to our BOP model, we employed the experimental value of E_c for hcp Co in our training set, and used DFT-derived values for relative energies only. Indeed, this strategy enabled our BOP model to predict the cohesive energy of hcp Co in near-perfect agreement with experiments (i.e., within 0.01 eV/atom; Table 2).

More importantly, our newly developed BOP parameters capture the energetic ordering, and relative energies (with respect to the most stable hcp phase) in excellent accordance with our DFT calculations (Table 2). It is important to note that since BOP interactions are limited to nearest neighbors alone, it cannot distinguish the energetic difference between hcp and fcc polymorphs of Co; this inherent deficiency of Tersoff-Brenner type BOP formalism has been reported for other metals.⁵³ Nevertheless, our BOP model describes the structure, and elastic properties of these phases accurately; furthermore, the computational efficiency afforded by the nearest-neighbor cut-off employed by BOP makes it a valuable tool to access long time-scales (tens of ns) and large length scales (multi-million atoms) necessary to study hybrid metal-organic porous materials.

Our newly-developed BOP model provides an accurate description of structure, and elastic properties of the various polymorphs of Co. As shown by Table 2, the BOP predicted lattice parameters are in excellent accordance with those obtained from DFT calculations, and previous experiments (within 2%). Similarly, the elastic constants Co polymorphs predicted by our newly developed BOP match well both with our DFT calculations, and available experiments. Furthermore, the equation of state (i.e., energy-volume dependence) of the Co polymorphs predicted by BOP agree well with those obtained from DFT calculations (Figure 2).

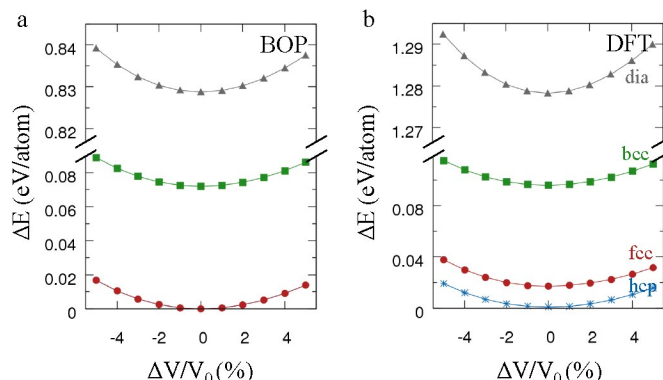


Fig. 2 Equation of state of different phases of Co, namely hcp (blue stars), fcc (red circles), bcc (green squares), and diamond cubic (gray triangles) calculated using (a) BOP parameters developed in this study, and (b) DFT calculations. The energy (ΔE) for each crystalline phase (provided in eV per unit formula, i.e. eV/u.f.) is relative to the cohesive energy of the most stable phase (i.e., hcp) at equilibrium as evaluated by the corresponding level of theory. Also, the volumetric strain ($\Delta V/V_0$) is determined with respect to the volume of a given phase at equilibrium as determined by a particular level of theory. In the framework of BOP, in which the interactions are limited to nearest neighbors, hcp and fcc phases are energetically indistinguishable (see text).

In addition to the bulk properties of Co phases, we test the performance of our BOP in predicting surface properties, which were not part of the training set. Table 3 compares the energies of low index surfaces of hcp (i.e., (0001) and (1010) and fcc Co (i.e., (111), (100), and (110)) predicted by BOP with those derived from our DFT calculations. The BOP predicted surface energies are in close agreement with the corresponding DFT values; importantly, the energetic ordering of the surfaces match exactly with DFT calculations.

While no stable crystalline compound exists in the Co-C binary system under standard conditions, previous electron microscopy and *in situ* X-ray studies have reported the formation of a metastable Co_2C phase (orthorhombic; $Pmnm$ space group), which possibly deactivates Co catalysts during Fischer-Tropsch

Table 3 Energies of low-index surfaces of hcp and fcc Co computed using BOP developed in this work, and DFT calculations. All the surface energies are provided in units of J/m².

Surface	BOP	DFT
Hexagonal close-packed		
(0001)	2.01	2.12
(1010)	2.82	2.26
Face centered cubic		
(111)	2.01	2.03
(100)	2.35	2.39
(110)	2.46	2.45

Table 4 Comparison of lattice parameters, heat of formation, and elastic constants of orthorhombic Co₂C predicted with the BOP model developed in this work with those obtained from DFT calculations.

	BOP	DFT
Structure		
<i>a</i> (Å)	2.87	2.88
<i>b</i> (Å)	4.36	4.37
<i>c</i> (Å)	4.36	4.37
ΔH (eV/u.f.)	0.41	0.33
Elastic constants (in GPa)		
<i>C</i> ₁₁	414	414
<i>C</i> ₁₂	177	176
<i>C</i> ₁₃	183	182
<i>C</i> ₂₂	346	361
<i>C</i> ₂₃	177	201
<i>C</i> ₃₃	349	340
<i>C</i> ₄₄	167	101
<i>C</i> ₅₅	122	149

synthesis.^{55–57} Our newly developed BOP model accurately captures the energetics, structure, and elastic properties of this phase, as shown by Table 4. Our BOP model predicts the formation of Co₂C from hcp Co and graphite to be endothermic (ΔH = 0.41 eV/u.f.) indicating that Co₂C is metastable; this is consistent with our DFT calculations (ΔH = 0.33 eV/u.f.) and experiments.^{55–57} Similar to the pure Co phases, the BOP model developed in this work describes the structure of Co₂C in excellent agreement with DFT calculations; the BOP predicted lattice parameters are within ~2% of the DFT values (Table 4). In addition, the elastic stiffness values of Co₂C obtained from the model show minor deviations from those derived from DFT calculations; the errors associated with BOP predictions, ~15%, are similar to the expected errors in the DFT-PBE framework itself.⁸¹

3.2 Self assembly of metal-organic porous networks

There is a lot of recent effort on directed synthesis of microscopic conducting materials which might provide low-cost, energy efficient, large-area, miniaturized, flexible and lightweight devices as an alternative for macroscopic wires in micro and nanoelectronics applications. As device features are pushed towards the nanometer regime, the continued increase in the device density of integrated circuits depends on miniaturization of the constituent components. Towards this end, our recently discovered optically directed patterning of electrically conductive hybrid mesoscopic surface architectures from organic and inorganic nanoparticles has the ability to synthesize electronic components that are mechanically soft yet electrically conductive.³⁷ The underlying molecular scale mechanism of directed assembly is not completely understood. Here, we simulate a prototypical binary mixture of

monodispersed Co₅₁₅ clusters and C₆₀ at various C/Co ratios (*f* = 0.086, 0.429, and 4.292) and evaluate the structural evolution of the hybrid architecture as a function of the relative composition of the nanoparticles. In particular, we seek to understand the composition dependent formation of continuous conducting pathways in the assembled structure as well as the mechanical properties of such structures.

During the 1 ns equilibration, we observe that 100 Co₅₁₅ clusters self-assemble into chains and branched structures depending on the relative number of C₆₀ present in the system (Figure 3 a-c). A higher connectivity between Co₅₁₅ clusters is observed at a lower C/Co ratio (Figure 3 d-f). The analysis of branched structures in a large 3D system consisting of a few million atoms is, in general, challenging. Here, we apply an unsupervised machine learning approach to enable a fast and automatic way of identifying individual connected Co structures, as well as obtaining an estimate of their sizes (occupied volume). The identification is done using a local-density-based clustering algorithm that assigns a Co atom to a nearby group of Co atoms if it has a minimum of 12 Co neighbors within a neighborhood cutoff of 3.2 Å. As shown by different colors in Figure 3 d-f, we have identified structures including a large branch of 49,000 Co atoms when *f* = 0.086, 5–12 nm long chains of up to 3,000 Co atoms when *f* = 0.429, and < 5 nm chains of ~480 Co atoms when *f* = 4.292. These results show a systematic increase in the length of self-assembled Co chains as the C/Co ratio is decreased. It is therefore expected that the formation of long Co chains and therefore improved electrical conduction will occur at an intermediate C/Co ratio between *f* = 0.086 and 0.429. This composition dependency is, thus, important for the design of flexible materials with tunable electrical conductivity.

We also evaluate the porosity of our simulated Co-C systems at various C/Co ratios. The voids between Co and C are mapped by voxelizing the simulation box using voxels with side length of 4 Å. The void structure analysis is done using the same clustering algorithm described in the Co connectivity analysis, but the clustering criterion is changed to a minimum of 27 neighbors within a neighborhood cutoff of 9 Å. The distribution plots (Figure 3 g-h) as a function of void sizes are obtained by accumulating data over the last 50 ps of the simulations, which show the probable size of voids to be ~779 nm³ when *f* = 0.086 and ~2,294 nm³ when *f* = 0.429. A higher porosity for mixtures with a higher C/Co ratio suggests that the addition of C₆₀ promote the formation of individual Co chains in place of compact Co structures.

We also evaluate the porosity of our simulated Co-C systems at various C/Co ratios. The voids between Co and C are mapped by voxelizing the simulation box using voxels of side length of 4 Å. Void structure analysis is accomplished using the same clustering algorithm described in the Co connectivity analysis, but the clustering criterion is changed to a minimum of 27 neighbors within a neighborhood cutoff of 9 Å. The distribution plots (Figure 3 g-h) as a function of void sizes are obtained by accumulating data over the last 50 ps of the simulations, which show the probable size of voids to be ~779 nm³ when *f* = 0.086 and ~2,294 nm³ when *f* = 0.429. A higher porosity for mixtures with a higher C/Co ratio suggests that the addition of C₆₀ promote the formation of

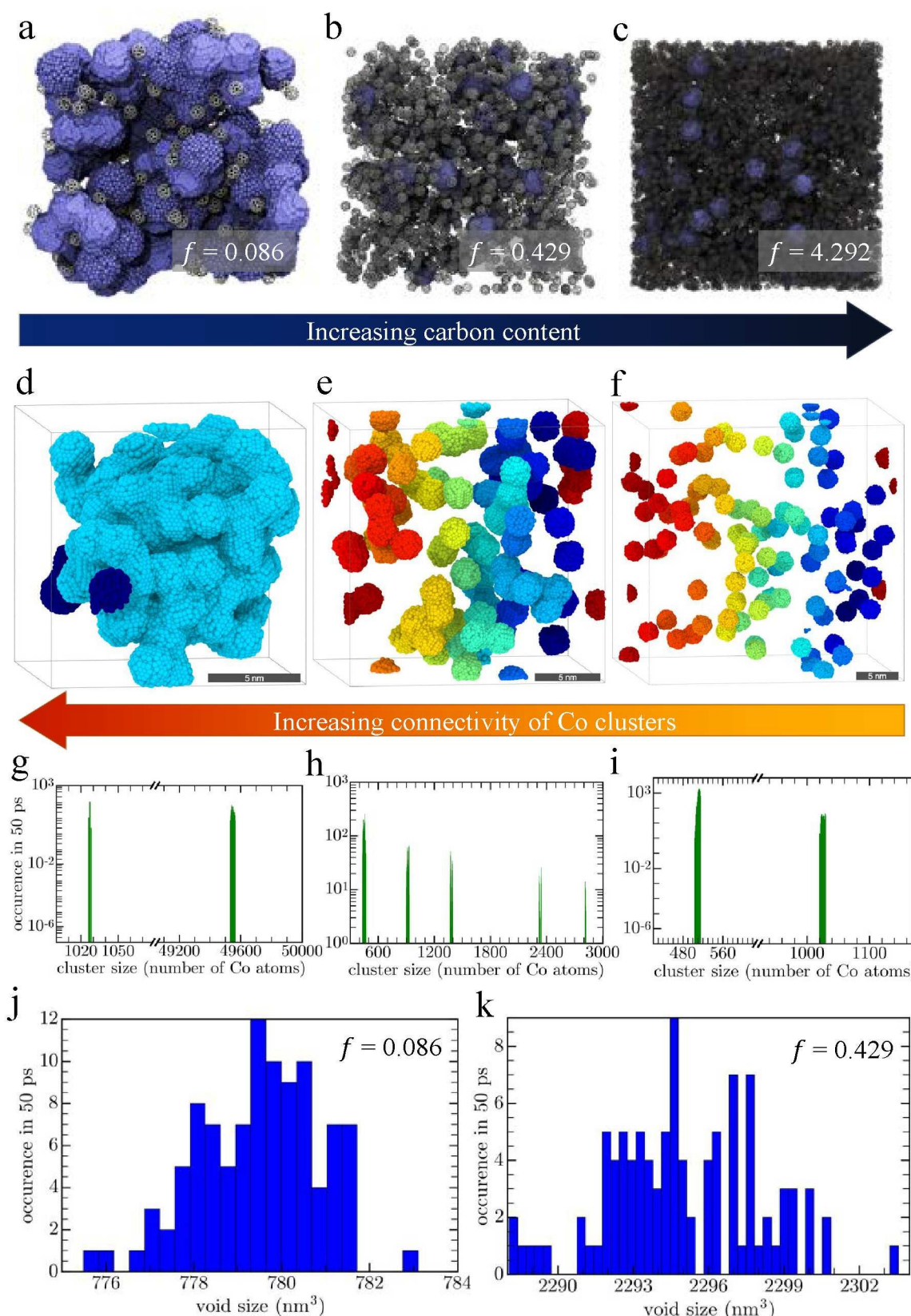


Fig. 3 Molecular dynamics simulations of self-assembly of Co₅₁₅ clusters and C₆₀ at 800 K. (a-c) Final configurations of the porous heterostructures at various C/Co ratios obtained from our MD simulations. The Co and C atoms are depicted as blue and grey spheres, respectively. (d-f) Chain/branched structures of Co₅₁₅ clusters identified using a clustering algorithm. Individual clusters are labeled by different colors. (g-h) Distribution plots showing the probable sizes of void in the low C/Co ratio systems. The histogram data is accumulated over the last 50 ps of each simulation.

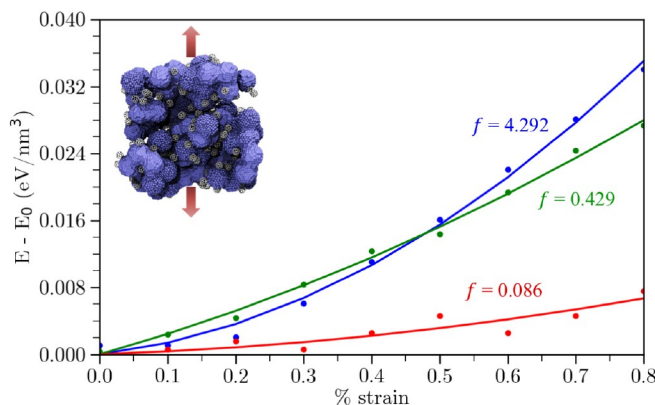


Fig. 4 Total energy of self-assembled heterostructures of Co₅₁₅ clusters and C₆₀ fullerenes as a function of applied strain, as evaluated using the BOP model developed in this work. For these computations, we employ the final configurations from our MD simulations (shown in Figs. 3 (a-c)) at various C/Co ratios.

individual Co chains in place of compact Co structures.

We further assess the mechanical stability of the hybrid assembled structures by computing their Young's modulus. As shown in Figure 4, we find that the system with higher Co composition ($f = 0.086$) has a higher Young's modulus (6.88 MPa) and is significantly stiffer than systems rich in carbon (2.43 MPa for $f = 0.429$ and 1.11 MPa for $f = 4.292$). This suggests that one can optimize the relative compositions of Co and C to achieve the desired combination of conductivity and stiffness for applications such as flexible electronics.

4 Conclusions

In summary, we have developed a machine learnt model for the cobalt-carbon inorganic-organic heterostructured system. Our machine learning strategy involves the use of supervised learning, i.e. genetic algorithms, followed by the simplex method to rigorously train a model based on bond order formalism against a first-principles based training data-set for various polymorphs of Co, Co-C and C. Our developed model successfully describes the energetics, structure, and elastic properties of pure components i.e. cobalt and carbon, as well as cobalt carbide (Co₂C) within a single bond-order framework. We apply our machine learnt model to perform large-scale molecular dynamics simulations to study the high temperature assembly of Co nanoparticles and fullerenes. Our large scale MD simulations model the assembly process for several different compositions from Co-rich to C-rich hybrids. Our model successfully predicts the strong composition dependence of both the structure and property of the assembled hybrid material. We find that Co-rich heterosystems result in a hybrid structure with a well-connected metallic network (i.e. such conduction pathways will translate to excellent electrical properties). On the other hand, C-rich assembled hybrids have poor metallic connectivity with high porosity and likely to have poor electrical conductivity. The Co-rich heterosystems are, however, much stiffer compared to C-rich hybrids. Simulations performed with an intermediate composition suggests an decrease in stiffness of the assembled hybrid with increasing C

composition and increased metallic contact as well as reduced porosity with increasing Co composition. Our simulation model can thus be used as a tool for optimizing the composition of the hybrid to achieve the desired mechanical and electrical properties in applications such as flexible electronics. The results of the developed models are in good agreement with recent experimental results on directed assembly of inorganic-organic hybrids. Our machine learnt potential model as well as the general training strategy outlined in this work can be broadly applied to model other inorganic-organic heterostructures within a single potential formalism. Such models could be used to investigate the atomistic mechanisms involved in self/directed assembly of hybrid materials as well as to understand the structure-property relationships of such hybrid structures.

Acknowledgements

Use of the Center for Nanoscale Materials, an Office of Science user facility, was supported by the U. S. Department of Energy, Office of Science, Office of Basic Energy Sciences, under Contract No. DE-AC02-06CH11357. This research used resources of the National Energy Research Scientific Computing Center, a DOE Office of Science User Facility supported by the Office of Science of the U.S. Department of Energy under Contract No. DE-AC02-05CH11231. An award of computer time was provided by the Innovative and Novel Computational Impact on Theory and Experiment (INCITE) program. This research used resources of the Argonne Leadership Computing Facility, which is a DOE Office of Science User Facility supported under Contract DE-AC02-06CH11357. We gratefully acknowledge the computing resources provided on Blues, a high-performance computing cluster operated by the Laboratory Computing Resource Center at Argonne National Laboratory.

References

- R. O. Ritchie, *Nat. Mater.*, 2011, **10**, 817–822.
- C. Gu and J.-S. Lee, *ACS Nano*, 2016, **10**, 5413–5418.
- J. T. Bahns, S. K. R. S. Sankaranarayanan, N. C. Giebink, H. Xiong and S. K. Gray, *Advanced Materials*, 2012, **24**, OP242–OP246.
- Y.-W. Li, L.-Y. Guo, H.-F. Su, Jagodič, M. Luo, X.-Q. Zhou, S.-Y. Zeng, C.-H. Tung, D. Sun and L.-S. Zheng, *Inorg. Chem.*, 2017, **56**, 2481–2489.
- A. P. Wight and M. E. Davis, *Chemical Reviews*, 2002, **102**, 3589–3614.
- F. Hoffmann, M. Cornelius, J. Morell and M. Fröba, *Angewandte Chemie International Edition*, 2006, **45**, 3216–3251.
- C. R. Kagan, D. B. Mitzi and C. D. Dimitrakopoulos, *Science*, 1999, **286**, 945–947.
- J. T. Bahns, S. K. R. S. Sankaranarayanan, S. K. Gray and L. Chen, *Phys. Rev. Lett.*, 2011, **106**, 095501.
- P. Judeinstein and C. Sanchez, *J. Mater. Chem.*, 1996, **6**, 511–525.
- C. Sanchez, B. Julian, P. Belleville and M. Popall, *J. Mater. Chem.*, 2005, **15**, 3559–3592.
- U. Schubert, N. Hüsing and A. Lorenz, *Chem. Mater.*, 1995, **7**,

- 2010–2027.
- 12 C. Sanchez, P. Belleville, M. Popall and L. Nicole, *Chem. Soc. Rev.*, 2011, **40**, 696–753.
- 13 F. Mammeri, E. L. Bourhis, L. Rozes and C. Sanchez, *J. Mater. Chem.*, 2005, **15**, 3787–3811.
- 14 A. Zamboulis, N. Moitra, J. J. E. Moreau, X. Cattoen and M. Wong Chi Man, *J. Mater. Chem.*, 2010, **20**, 9322–9338.
- 15 Y.-P. Zhu, T.-Y. Ma, Y.-L. Liu, T.-Z. Ren and Z.-Y. Yuan, *Inorg. Chem. Front.*, 2014, **1**, 360–383.
- 16 L. Nicole, C. Boissiere, D. Gross, A. Quach and C. Sanchez, *J. Mater. Chem.*, 2005, **15**, 3598–3627.
- 17 A. Li, H. Shen, H. Ren, C. Wang, D. Wu, R. A. Martin and D. Qiu, *J. Mater. Chem. B*, 2015, **3**, 1379–1390.
- 18 L. M. Gordon and D. Joester, *Nature*, 2011, **469**, 194–197.
- 19 A. Kaushik, R. Kumar, S. K. Arya, M. Nair, B. D. Malhotra and S. Bhansali, *Chemical Reviews*, 2015, **115**, 4571–4606.
- 20 M. Vallet-Regi, M. Colilla and B. Gonzalez, *Chem. Soc. Rev.*, 2011, **40**, 596–607.
- 21 P. Verma, P. Maire and P. Novak, *Electrochim Acta*, 2010, **55**, 6332–6341.
- 22 K. Leung, F. Soto, K. Hankins, P. B. Balbuena and K. L. Harrison, *The Journal of Physical Chemistry C*, 2016, **120**, 6302–6313.
- 23 M. Wright and A. Uddin, *Solar Energy Materials and Solar Cells*, 2012, **107**, 87–111.
- 24 K. Nomura, H. Ohta, A. Takagi, T. Kamiya, M. Hirano and H. Hosono, *Nature*, 2004, **432**, 488–492.
- 25 W. Baaziz, S. Begin-Colin, B. P. Pichon, I. Florea, O. Ersen, S. Zaferatos, R. Barbosa, D. Begin and C. Pham-Huu, *Chem. Mater.*, 2012, **24**, 1549–1551.
- 26 S. Dou, X. Li, L. Tao, J. Huo and S. Wang, *Chem. Commun.*, 2016, **52**, 9727–9730.
- 27 D. Ji, S. Peng, D. Safanama, H. Yu, L. Li, G. Yang, X. Qin, M. Srinivasan, S. Adams and S. Ramakrishna, *Chemistry of Materials*, 2017, **29**, 1665–1675.
- 28 S. Liu, Z. Wang, S. Zhou, F. Yu, M. Yu, C.-Y. Chiang, W. Zhou, J. Zhao and J. Qiu, *Advanced Materials*, 2017, 1700874–n/a.
- 29 M. Kurmoo, *Chem. Soc. Rev.*, 2009, **38**, 1353–1379.
- 30 G. L. Bezemer, J. H. Bitter, H. P. C. E. Kuipers, H. Oosterbeek, J. E. Holewijn, X. Xu, F. Kapteijn, A. J. van Dillen and K. P. de Jong, *Journal of the American Chemical Society*, 2006, **128**, 3956–3964.
- 31 W. Raróg-Pilecka, E. Miśkiewicz, M. Matyszek, Z. Kaszkur, L. Kępiński and Z. Kowalczyk, *Journal of Catalysis*, 2006, **237**, 207–210.
- 32 D. S. Bethune, C. H. Klang, M. S. de Vries, G. Gorman, R. Savoy, J. Vazquez and R. Beyers, *Nature*, 1993, **363**, 605–607.
- 33 D. Berman, S. A. Deshmukh, S. K. Sankaranarayanan, A. Erdemir and A. V. Sumant, *Science*, 2015, **348**, 1118–1122.
- 34 A. Erdemir, G. Ramirez, O. L. Eryilmaz, B. Narayanan, Y. Liao, G. Kamath and S. K. Sankaranarayanan, *Nature*, 2016, **536**, 67–71.
- 35 B. Narayanan, S. A. Deshmukh, S. K. Sankaranarayanan and S. Ramanathan, *Electrochimica Acta*, 2015, **179**, 386–393.
- 36 S. M. Foiles, M. I. Baskes and M. S. Daw, *Phys. Rev. B*, 1986, **33**, 7983–7991.
- 37 J. Tersoff, *Phys. Rev. B*, 1988, **37**, 6991–7000.
- 38 J. Tersoff, *Phys. Rev. B*, 1989, **39**, 5566–5568.
- 39 D. W. Brenner, O. A. Shenderova, J. A. Harrison, S. J. Stuart, B. Ni and S. B. Sinnott, *Journal of Physics: Condensed Matter*, 2002, **14**, 783.
- 40 A. I. Skouidas and D. S. Sholl, *The Journal of Physical Chemistry B*, 2005, **109**, 15760–15768.
- 41 Y. Shibuta and S. Maruyama, *Computational Materials Science*, 2007, **39**, 842–848.
- 42 B. Narayanan, A. Kinaci, F. G. Sen, M. J. Davis, S. K. Gray, M. K. Chan and S. K. Sankaranarayanan, *The Journal of Physical Chemistry C*, 2016, **120**, 13787–13800.
- 43 M. Backman, N. Juslin and K. Nordlund, *The European Physical Journal B*, 2012, **85**, 317.
- 44 K. Chenoweth, A. C. T. van Duin and W. A. Goddard, *The Journal of Physical Chemistry A*, 2008, **112**, 1040–1053.
- 45 K. D. Nielson, A. C. T. van Duin, J. Oxgaard, W.-Q. Deng and W. A. Goddard, *The Journal of Physical Chemistry A*, 2005, **109**, 493–499.
- 46 E. C. Neyts, Y. Shibuta, A. C. T. van Duin and A. Bogaerts, *ACS Nano*, 2010, **4**, 6665–6672.
- 47 D. W. Brenner, *Phys. Rev. B*, 1990, **42**, 9458–9471.
- 48 M. Müller, P. Erhart and K. Albe, *J. Phys. Cond. Matt.*, 2007, **19**, 326220.
- 49 B. Narayanan, K. Sasikumar, Z.-G. Mei, A. Kinaci, F. G. Sen, M. J. Davis, S. K. Gray, M. K. Y. Chan and S. K. R. S. Sankaranarayanan, *The Journal of Physical Chemistry C*, 2016, **120**, 17475–17483.
- 50 K. Sasikumar, B. Narayanan, M. Cherukara, A. Kinaci, F. G. Sen, S. K. Gray, M. K. Y. Chan and S. K. R. S. Sankaranarayanan, *Chemistry of Materials*, 2017, **29**, 3603–3614.
- 51 M. J. Cherukara, B. Narayanan, A. Kinaci, K. Sasikumar, S. K. Gray, M. K. Chan and S. K. R. S. Sankaranarayanan, *The Journal of Physical Chemistry Letters*, 2016, **7**, 3752–3759.
- 52 F. G. Sen, A. Kinaci, B. Narayanan, S. K. Gray, M. J. Davis, S. K. R. S. Sankaranarayanan and M. K. Y. Chan, *J. Mater. Chem. A*, 2015, **3**, 18970–18982.
- 53 P. Erhart, N. Juslin, O. Goy, K. Nordlund, R. Müller and K. Albe, *J. Phys. Cond. Matt.*, 2006, **18**, 6585.
- 54 N. Juslin, P. Erhart, P. Träskelin, J. Nord, K. O. E. Henriksson, K. Nordlund, E. Salonen and K. Albe, *J. Appl. Phys.*, 2005, **98**, 123520.
- 55 O. Ducreux, J. Lynch, B. Rebours, M. Roy and P. Chaumette, *Studies in Surface Science and Catalysis*, 1998, **119**, 125–130.
- 56 F. Tihay, A. Roger, A. Kiennemann and G. Pourroy, *Catalysis Today*, 2000, **58**, 263–269.
- 57 F. Tihay, G. Pourroy, M. Richard-Plouet, A. Roger and A. Kiennemann, *Applied Catalysis A: General*, 2001, **206**, 29–42.
- 58 Y.-H. Zhao, H.-Y. Su, K. Sun, J. Liu and W.-X. Li, *Surface Science*, 2012, **606**, 598–604.
- 59 G. Kresse and J. Furthmüller, *Comp. Mat. Sci.*, 1996, **6**, 15–50.

- 60 G. Kresse and J. Furthmuller, *Phys. Rev. B*, 1996, **54**, 11169–11186.
- 61 J. P. Perdew, K. Burke and M. Ernzerhof, *Phys. Rev. Lett.*, 1996, **77**, 3865–3868.
- 62 K. Sastry, D. E. Goldberg and G. Kendall, *Search Methodologies: Introductory Tutorials in Optimization and Decision Support Techniques*, Springer, Berlin, 2005, ch. 4, pp. 93–117.
- 63 W. H. Press, S. A. Teukolsky, W. T. Vetterling and B. P. Flannery, *Numerical Recipes: The Art of Scientific Computing*, Cambridge University Press, New York, USA, 3rd edn, 2007.
- 64 S. Plimpton, *J. Comput. Phys.*, 1995, **117**, 1–19.
- 65 K. Deb and R. B. Agrawal, *Complex Systems*, 1995, **9**, 115–148.
- 66 D. E. Goldberg, *Genetic Algorithms in Search Optimization and Machine Learning*, Addison-Wesley, Reading, MA, 1989.
- 67 K. Deb, *Multi-Objective Optimization Using Evolutionary Algorithms*, John Wiley and Sons, Chichester, UK, 2001.
- 68 K. Deb and S. M. T. Pratap, A. Agarwal, *Trans. Evol. Comp*, 2002, **6**, 182–197.
- 69 C. Kittel, *Introduction to Solid State Physics*, Wiley-Interscience, New York, 1986.
- 70 W. B. Pearson, *Handbook of Lattice Spacings and Structure of Metals and Alloys*, Vol. 2, Pergamon Press Ltd., Oxford, England, 1967.
- 71 G. Simmons and W. H., *Single Crystal Elastic Constants and Calculated Aggregate Properties*, MIT Press, Cambridge, MA, 1977.
- 72 T. Nishizawa and K. Ishida, *Bulletin of Alloy Phase Diagrams*, 1983, **4**, 387–390.
- 73 *CRC Handbook of Chemistry and Physics*, ed. D. R. Lide and W. M. M. Haynes, CRC, Boca Raton, FL, 2009.
- 74 *Elastic, Piezoelectric, Pyroelectric, Piezooptic, Electrooptic Constants and Nonlinear Dielectric Susceptibilities of Crystals in Landolt-Börnstein Numerical Data and Functional Relationships in Science and Technology, New Series, Group III, Crystal and Solid State Physics*, ed. K. H. Hellwege and A. M. Hellwege, vol. 11.
- 75 S. M. Wild, J. Sarich and N. Schunck, *Journal of Physics G: Nuclear and Particle Physics*, 2015, **42**, 034031.
- 76 B. Narayanan, I. E. Reimanis, E. R. Fuller and C. V. Ciobanu, *Phys. Rev. B*, 2010, **81**, 104106.
- 77 B. Narayanan, A. C. T. van Duin, B. B. Kappes, I. E. Reimanis and C. V. Ciobanu, *Modelling and Simulation in Materials Science and Engineering*, 2012, **20**, 015002.
- 78 D. C. Wallace, *Thermodynamics of crystals*, Wiley, New York, USA, 1972.
- 79 L. Schimka, R. Gaudoin, J. c. v. Klimeš, M. Marsman and G. Kresse, *Phys. Rev. B*, 2013, **87**, 214102.
- 80 M. R. LaBrosse, J. K. Johnson and A. C. T. van Duin, *J. Phys. Chem. A*, 2010, **114**, 5855–5861.
- 81 K. Lejaeghere, V. van Speybroek, G. van Oost and S. Cottenier, *Critical Reviews in Solid State and Materials Sciences*, 2014, **39**, 1–24.

Nanoscale

Page 12 of 12